SCIENCE CHINA
Physics, Mechanics & Astronomy

• Research Paper •

March 2011 Vol.54 No.3: 511–522
doi: 10.1007/s11433-010-4220-x

A 5th order monotonicity-preserving upwind compact difference scheme

HE ZhiWei[1], LI XinLiang[1*], FU DeXun[2] & MA YanWen[2]

[1] *The Key Laboratory of High Temperature Gas Dynamics, Institute of Mechanics, Chinese Academy of Sciences, Beijing 100190, China;*
[2] *The State Key Laboratory of Nonlinear Mechanics, Institute of Mechanics, Chinese Academy of Sciences, Beijing 100190, China*

Received July 22, 2010; accepted November 19, 2010; published online January 18, 2011

Based on an upwind compact difference scheme and the idea of monotonicity-preserving, a 5th order monotonicity-preserving upwind compact difference scheme (m-UCD5) is proposed. The new difference scheme not only retains the advantage of good resolution of high wave number but also avoids the Gibbs phenomenon of the original upwind compact difference scheme. Compared with the classical 5th order WENO difference scheme, the new difference scheme is simpler and small in diffusion and computation load. By employing the component-wise and characteristic-wise methods, two forms of the new difference scheme are proposed to solve the N-S/Euler equation. Through the Sod problem, the Shu-Osher problem and the two-dimensional Double Mach Reflection problem, numerical solutions have demonstrated this new scheme does have a good resolution of high wave number and a robust ability of capturing shock waves, leading to a conclusion that the new difference scheme may be used to simulate complex flows containing shock waves.

upwind compact scheme, monotonicity-preserving, compressible flows, shock capturing scheme

PACS: 47.11.Bc, 7.40.Ki, 47.40.Nm

1 Introduction

One of the great challenges in aerospace industries is the technology of numerically simulating compressible complex flows. Yet such flows are often mixed with many complex factors, such as turbulence, shock waves, and separated flows. They may also take on many complicated features, including multi-scale structures and strong discontinuities, while different kinds of waves are simultaneously playing different roles. For a detailed portrayal of such flows, high order schemes are applied, because they can resolve smaller structures in the same condition owing to their fewer dissipation and dispersion errors.

A good scheme should be able to obtain a sharp and vivid picture of the solution to the original physical problem, which is commonly called high-resolution scheme [1]. According to this definition, a high resolution scheme should genuinely have the following features [2]: (1) to have 2nd or higher order accuracy in smooth parts of the solution; (2) to produce numerical solutions free from spurious oscillation; (3) to produce a high-resolution of discontinuities, that is, the number of mesh points in the transition zone containing the numerical wave is narrow in comparison with that of the first-order monotone methods. So high-order doesn't mean high-resolution. In 1983, Harten [1] introduced the concept of total variation diminishing (TVD), and got a 2nd order TVD scheme by treating the numerical flux of the 1st order upwind scheme with the anti-diffusion method. Based on Harten's TVD concept and its sufficient condition [1] as well as the idea of using limiters [1], Sweby [3] proposed using the flux limiters to construct a series of 2nd order TVD schemes. In addition, Van Leer [4] put forward a method called MUSCL (monotonic upstream-centered scheme for conservation law) to first interpolate interface

*Corresponding author (email: lixl@imech.ac.cn)

values by using the known cell averages, then to limit the interface value probably, and in the end, to use the flux vector splitting (FVS) method to obtain a scheme with good dispersion and diffusion characteristics and high-resolution of shocks. Henceforth, in the 1980s, researchers proposed a variety of TVD schemes, such as NND [5]. For the shock capturing, the TVD schemes have been confirmed to be reliable and effective. But in order to satisfy the mathematical property that the total variation does not increase, the order of all TVD schemes degenerates to first-order at local extreme points. To avoid this drawback, Harten et al. [6] introduced the concept of essentially non-oscillatory (ENO), allowing schemes to cause high-order false fluctuation. Since then, many researchers have constructed concrete high-order ENO [6,7] schemes and weighted ENO [7,8] schemes. There also are the total variation bounded (TVB) [9] method and monotonicity-preserving (MP) [10] method.

Generally speaking, compact schemes can be classified into two categories: centered (see in ref. [11]) and upwind (see in ref. [12]). As one kind of high order scheme, the advantage of compact schemes is obvious. Using the same stencils, compact schemes can get higher accuracy, higher resolution with fewer dissipation and dispersion errors compared to the traditional ones. But the compact schemes also run into the problem of spurious oscillations. And the higher the order is, the more difficult the oscillations are to be overcome. Halt et al. [13] thought the further development of the compact schemes lies in the research of the shock-capturing technology. To capture shocks robustly, treating the compact schemes nonlinearly is required. However, so far, there are not many remarkable results except the following:

(1) Cockburn and Shu [14] proposed 3rd and 4th order compact nonlinear schemes based on TVD and TVB concepts, but the solutions near shock waves oscillate obviously for the 4th schemes.

(2) Ravichandran [15] constructed high order compact schemes by applying the minmod flux limiter to the high order compact difference. But the schemes degenerate to the 1st in the vicinity of shocks and extreme points.

(3) Adams and Shariff [16], Pirozzoli [17], Ren et al. [18] developed respectively the hybrid methods in which the non-oscillatory shock capturing schemes are only used locally near the discontinuities and the compact schemes are used in smooth regions. However, the weight function which abrupts transition from one sub-scheme to another includes experience parameters.

(4) Deng and Zhang [19] proposed a kind of nonlinear compact scheme. These schemes achieve high-order accuracy by cell-centered compact schemes and compact high-order interpolations at cell-edges by using ENO or WENO reconstruction methods. However, the computational cost of this scheme is high.

(5) Ma and Fu [20] proposed a 4th order accurate compact scheme with group velocity control by using the group velocity control method. This scheme is small in computation load, but it needs to distinguish the front and back of shocks, which is hard to achieve. As a result, the scheme can't capture shocks robustly.

In this paper, we propose a 5th order monotonicity-preserving upwind compact difference scheme (m-UCD5). Following the component-wise and characteristic-wise methods, we apply the new difference scheme to solving the N-S/Euler equation.

2 Numerical methodology

2.1 The scalar conservation law

Consider the scalar hyperbolic conservation law given by

$$\frac{\partial u}{\partial t}+\frac{\partial f(u)}{\partial x}=0. \tag{1}$$

Let $\{I_j\}$ be a uniform partition of the solution domain in space, where $I_j=\left[x_{j-1/2},x_{j+1/2}\right]$ and $x_{j+1/2}-x_{j-1/2}=h$.

The semi-discrete conservative finite difference of (1) can be written as

$$\frac{\partial u}{\partial t}+\frac{1}{h}(\hat{f}_{j+1/2}-\hat{f}_{j-1/2})=0, \tag{2}$$

where $\hat{f}_{j+1/2}$ is the numerical flux function. If

$$\frac{1}{h}(\hat{f}_{j+1/2}-\hat{f}_{j-1/2})=\left(\frac{\partial f}{\partial x}\right)_j+O(h^k), \tag{3}$$

this scheme is the *k*th order scheme. In the present work, the time integration is performed by means of a three-stage, TVD Runge-Kutta scheme [21]. Defining

$$L_j(u)=-\frac{1}{h}(\hat{f}_{j+1/2}-\hat{f}_{j-1/2}), \tag{4}$$

then this scheme is given by

$$\begin{aligned} u_j^{(1)}&=u_j^n+\Delta t\cdot L_j(u^n),\\ u_j^{(2)}&=\frac{3}{4}u_j^n+\frac{1}{4}u_j^{(1)}+\frac{1}{4}\Delta t\cdot L_j(u^{(1)}),\\ u_j^{n+1}&=\frac{1}{3}u_j^n+\frac{2}{3}u_j^{(2)}+\frac{2}{3}\Delta t\cdot L_j(u^{(2)}). \end{aligned} \tag{5}$$

2.2 Fu and Ma's 5th order upwind compact difference scheme

Compact schemes are generally prone to have relatively high order in a small stencil. Fu and Ma [22] proposed a 5th order upwind compact difference scheme (UCD5). Gener-

ally, the construction process of this scheme may be summarized as: first use a flux splitting method to split $f = f^+ + f^-$, satisfying $\frac{\mathrm{d}f^+}{\mathrm{d}u} \geqslant 0$, $\frac{\mathrm{d}f^-}{\mathrm{d}u} \leqslant 0$. And then get the scheme according to the following equations:

$$\frac{2}{5}F^+_{j-1} + \frac{3}{5}F^+_j = \frac{-3f^+_{j-2} - 44f^+_{j-1} + 36f^+_j + 12f^+_{j+1} - f^+_{j+2}}{60 \cdot h}, \quad (6a)$$

$$\frac{2}{5}F^-_{j+1} + \frac{3}{5}F^-_j = \frac{3f^-_{j+2} + 44f^-_{j+1} - 36f^-_j - 12f^-_{j-1} + f^-_{j-2}}{60 \cdot h}, \quad (6b)$$

where $F^\pm_j = \left(\frac{\partial f^\pm}{\partial x}\right)_j$.

In order to analyze quantitatively the dispersion and dissipation errors of the 1st order upwind difference scheme (1U), the 5th order upwind biased difference scheme (5U) and the 5th order upwind compact difference scheme (5UCD), we take

$$\text{equation: } \frac{\partial u}{\partial t} + a\frac{\partial u}{\partial x} = 0,\ a = \text{const} > 0,$$

$$\text{initial condition: } u(x,0) = \mathrm{e}^{\mathrm{i}kx},$$

$$\text{exact solution: } u(x,t) = \mathrm{e}^{\mathrm{i}k(x-at)},$$

as a model problem.

If we let F_j/h represent all kinds of difference expressions which are to approximate $\left(\frac{\partial u}{\partial x}\right)_j$, and suppose the solution has the form $u(x,t) = \hat{u}(t)\mathrm{e}^{\mathrm{i}kx}$, then we can get $F_j = k_e \cdot \hat{u}(t)\mathrm{e}^{\mathrm{i}kx_j}$, where $k_e = k_r + \mathrm{i}k_i$. So the exact solution to the semi-equation $\frac{\mathrm{d}u_j}{\mathrm{d}t} + a\frac{F_j}{h} = 0$ is $u(x_j,t) = \mathrm{e}^{-k_r\frac{at}{h}}\mathrm{e}^{\mathrm{i}(kx_j - ak_i\frac{1}{h}t)}$.

Note that for the exact solution, we have $k_r = 0$, $k_i = \alpha = kh$. So the dispersion and diffusion errors of different schemes can be reflected by the functions k_i and k_r [23]. In Figure 1, the dispersion and diffusion errors of the 1U, 5U and 5UCD schemes are presented. And it shows that the 5th order upwind compact difference scheme has higher resolution and less dissipation compared with the others.

Table 1 gives the maximal values of α corresponding to the k_i and k_r when they are not more than 5% and 2% of their exact solutions of 1U, 5U and 5UCD. Obviously we can conclude that the range of the wave number which the UCD5 can simulate correctly is larger than that of U5.

Moreover, such upwind compact difference schemes with a special feature, that is, the numerical flux, can be written as the "pseudo-explicit" form. That is to say, the numerical flux can be got by using the following recurrence relations when the numerical flux of the upwind adjacent point is already known.

$$\hat{f}^+_{j+\frac{1}{2}} = \frac{5}{3}\cdot\left[\left(\frac{3f^+_{j-1} + 47f^+_j + 11f^+_{j+1} - f^+_{j+2}}{60}\right) - \frac{2}{5}\cdot\hat{f}^+_{j-\frac{1}{2}}\right], \quad (7a)$$

$$\hat{f}^-_{j+\frac{1}{2}} = \frac{5}{3}\cdot\left[\left(\frac{3f^-_{j+2} + 47f^-_{j+1} + 11f^-_j - f^-_{j-}}{60}\right) - \frac{2}{5}\cdot\hat{f}^-_{j+\frac{3}{2}}\right]. \quad (7b)$$

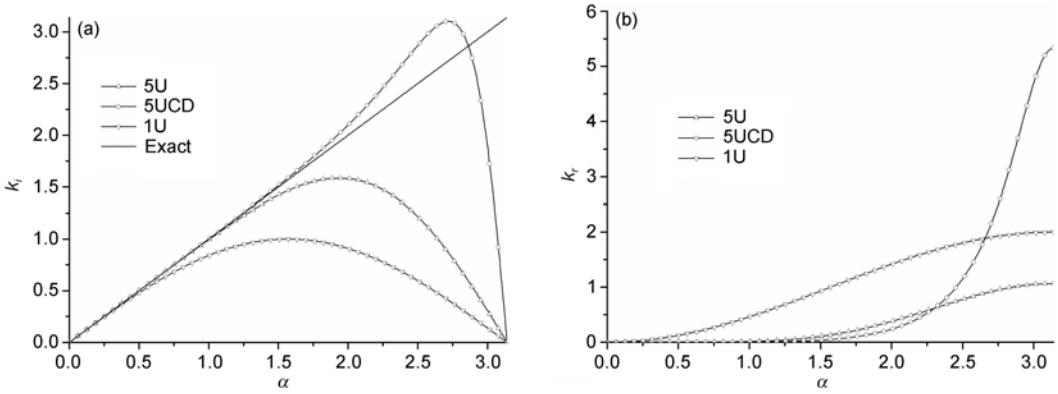

Figure 1 The modified wavenumber of 1U, 5U and 5UCD. (a) Imaginary part (dispersion); (b) real part (dissipation).

Table 1 The maximal values of α (α=kh) corresponding to k_i and k_r

	$k_r \leqslant 5\%$	$k_r \leqslant 2\%$	$(1-k_i/\alpha) \leqslant 5\%$	$(1-k_i/\alpha) \leqslant 2\%$
1U	0.318	0.201	0.552	0.348
5U	1.29	1.08	1.49	1.25
5UCD	1.57	1.35	2.01	1.71

As to the centered compact difference schemes, the multi-diagonal matrix inversion is required to get the numerical flux. Although the method of chase can be used to get the recurrence relations, it is usually bidirectional recurrence relation ("pursuing" process and "catching up" process). So the solving efficiency, especially the parallel efficiency is inferior to Fu and Ma's upwind compact difference scheme.

In a word, it is convenient to limit Fu and Ma's upwind compact difference scheme [22] due to its unidirectional recursive property.

2.3 Monotonicity preserving constraints

Given the scalar hyperbolic conservation equation with a constant speed, a "First-Order Accurate Constraint" method was proposed in ref. [10]. And in ref. [24], the authors demonstrated that this method is identical to the TVD method. In this paper, we will discuss the method generally, modify it for the semi-discrete scheme and apply it to Fu and Ma's upwind compact difference scheme [22].

Consider the scalar hyperbolic conservation eq. (1) with the speed satisfying $\frac{\mathrm{d}f}{\mathrm{d}u} = a = \text{const} > 0$. That is the case for $\hat{f}^{+}_{j+\frac{1}{2}}$. For the case $a < 0$ (i.e. $\hat{f}^{-}_{j-\frac{1}{2}}$), the method will be omitted due to symmetry.

The classical difference TVD schemes can be somewhat viewed as the results of correcting the 1st order upwind difference scheme. On the stencil $[x_{j-2}, x_{j-1}, x_j, x_{j+1}]$, the numerical flux can be written in the generic form:

$$\hat{f}_{j+\frac{1}{2}} = f_j + \frac{1}{\phi_T}\phi_{j+\frac{1}{2}}(r_{j+\frac{1}{2}}, \nu)\cdot(f_{j+1} - f_j), \tag{8}$$

where $\nu = a\cdot\frac{\tau}{h}$ is the CFL number, and

$$r_{j+\frac{1}{2}} = \frac{\Delta_{upw}}{\Delta_{loc}} = \frac{u^n_j - u^n_{j-1}}{u^n_{j+1} - u^n_j}.$$

And ϕ_T is the upper bound of the TVD limiters, i.e.

$$0 = \phi_B \leqslant \phi_{j+\frac{1}{2}} \leqslant \phi_T. \tag{9}$$

Following the criteria developed by Harten [1], we get another constraint:

$$0 \leqslant \left(\nu - \nu\frac{1}{\phi_T}\phi_{j-\frac{1}{2}}\right) + \frac{1}{\phi_T}\phi_{j+\frac{1}{2}}\frac{\nu}{r_{j+\frac{1}{2}}} \leqslant 1. \tag{10}$$

So, the general constrains for a one-step scheme to be TVD are

$$0 = \phi_B \leqslant \phi_{j+\frac{1}{2}} \leqslant \phi_T, \tag{11a}$$

$$0 \leqslant \phi_{j+\frac{1}{2}} \leqslant \phi_S = \phi_T\cdot\frac{1-\nu}{\nu}\cdot r_{j+\frac{1}{2}}. \tag{11b}$$

And the region satisfying the two equations above (11(a), 11(b)) is the TVD region (see Figure 2(a)).

Define

$$\gamma^{+} = \frac{1}{\phi_T}\cdot\phi_{j+\frac{1}{2}}(r_{j+\frac{1}{2}}, \nu), \tag{12a}$$

$$\gamma^{-} = \frac{1}{\phi_S}\cdot\phi_{j+\frac{1}{2}}(r_{j+\frac{1}{2}}, \nu). \tag{12b}$$

Eqs. (11a) and (11b) can be simplified as

$$0 \leqslant \gamma^{+} \leqslant 1, \tag{13a}$$

$$0 \leqslant \gamma^{-} \leqslant 1. \tag{13b}$$

Now we give a general definition:

$$f^{ul}_j = f_j + \kappa(r_{j+\frac{1}{2}}, \nu)\cdot(f_j - f_{j-1}), \tag{14}$$

where

$$\kappa(r_{j+\frac{1}{2}}, \nu) = \frac{\phi_S}{\phi_T\cdot r_{j+\frac{1}{2}}}.$$

Then eq. (8) can be rewritten as

$$\hat{f}_{j+\frac{1}{2}} = f_j + \gamma^{+}\cdot(f_{j+1} - f_j), \tag{15a}$$

$$\hat{f}_{j+\frac{1}{2}} = f_j + \gamma^{-}\cdot(f^{ul}_j - f_j). \tag{15b}$$

Taking account of eqs. (13a) and (13b), we have

$$f_{j+\frac{1}{2}} \in \left[f_j, f_{j+1}\right], \tag{16a}$$

$$\hat{f}_{j+\frac{1}{2}} \in \left[f_j, f^{ul}\right], \tag{16b}$$

where $\left[z_1, z_2, \cdots, z_k\right]$ represents the interval:

$$\left[\min(z_1, z_2, \cdots, z_k), \max(z_1, z_2, \cdots, z_k)\right].$$

That is to say, if the numerical flux lies in the two intervals above, the scheme is TVD. And in ref. [10], the parameter $\alpha = 4$ is identical to the function value $\alpha = \kappa(r_{j+\frac{1}{2}}, \nu = 0.2)$.

Finally, we analyze the method generally and give a simple modification.

(1) The order is not a factor in the process of constructing

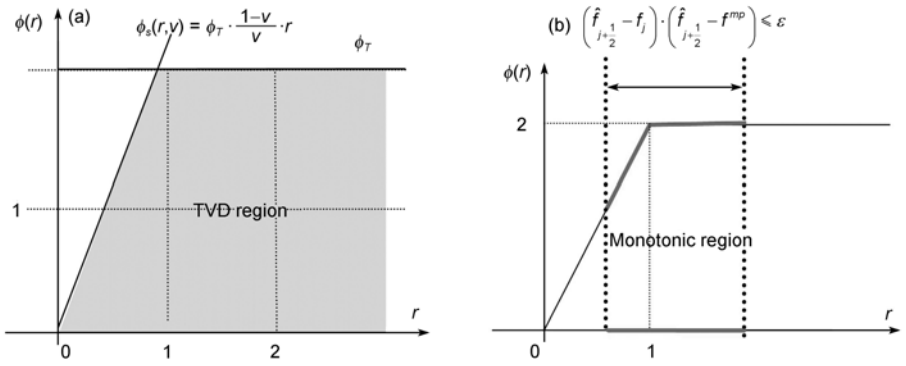

Figure 2 (a) The TVD region; (b) the switch function obtained by the TVD region.

monotoncity-preserving constraints. The essence of this method is to utilize the common TVD region to supply an interval in which the numerical flux $\hat{f}_{j+\frac{1}{2}}$ should lie in the monotonic part of the solution. And the upper/lower bound is f_{j+1} and f^{ul}, while the lower/upper bound is f_j. In the end, we can get a TVD interval $\left[f_a^{mp}, f_b^{mp}\right]$, while, following ref. [10], the upper and lower bounds are chosen as

$$f_a^{mp} = f_j,$$

$$f_b^{mp} = f_j + \min \mathrm{mod}(f_{j+1} - f_j, f^{ul} - f_j).$$

Furthermore, we can use the following inequality

$$(\hat{f}_{j+\frac{1}{2}} - f_a^{mp})(\hat{f}_{j+\frac{1}{2}} - f_b^{mp}) \leqslant \varepsilon$$

as a switch to distinguish the monotonic parts and the parts of extrema and discontinuities, where $\varepsilon = 10^{-10}$ in ref. [10]. Figure 2(b) shows this relation clearly.

(2) In the new definition of f_j^{ul}, the κ is no longer an experience parameter, but a general function $\kappa = \kappa(r, v)$.

(3) Ref. [25] mentioned a TVD condition $\phi(r) \leqslant \max(0, 2r)$ for the spatial discretization (ignoring any time-step restrictions). However, we intuitively think that the cases when $r \to +0$ and $r \to +\infty$ should be treated identically. As far as the symmetry is concerned, we get $\phi(r) = \min\left(\max(0, 2r), 2\right)$. Thus a semi-discrete monotonocity-preserving method (we call it modified monotonocity-preserving method) is obtained while the method of time integration is not always the three-stage, TVD Runge-Kutta scheme. Considering these, the κ simply is 1.

2.4 Accuracy-preserving

Similar to the classical TVD schemes, the method above causes the order of schemes to degenerate to 1st order in the vicinity of local extrema. In order to solve this problem, a great method was proposed in ref. [10], and modified later in ref. [24]. The idea of this method is to enlarge intervals defined above to avoid the loss of accuracy.

Enlarge the two intervals above to $\left[f_j, f_{j+1}, f^{md}\right]$, $\left[f_j, f^{ul}, f^{lc}\right]$, respectively, with

$$f^{md} = \frac{1}{2}(f_j + f_{j+1}) - \frac{1}{2} d^{MM}_{j+\frac{1}{2}}, \tag{17a}$$

$$f^{lc} = f_j + \frac{1}{2}(f_j - f_{j-1}) + \frac{8}{3} \cdot d^{MM}_{j-\frac{1}{2}}, \tag{17b}$$

a modification was given in ref. [24]:

$$f^{md} = \frac{1}{2}(f_j + f_{j+1}) - \frac{1}{2} d^{MM}_{j+\frac{1}{2}}, \tag{18a}$$

$$f^{lc} = f_j + \frac{1}{2}\left(1 + \frac{d^{MM}_{j-\frac{1}{2}}}{f_j - f_{j-1}}\right) \cdot (f^{ul} - f_j), \tag{18b}$$

and a conclusion was demonstrated mathematically that the modified f^{md} and f^{lc}, in the monotonic parts, satisfy:

$$f^{md} \in \left[f_j, f_{j+1}\right], \tag{19a}$$

$$f^{lc} \in \left[f_j, f^{ul}\right]. \tag{19b}$$

In this paper, we redefine two parameters:

$$f^{md} = \frac{1}{2}(f_j + f_{j+1}) - \frac{1}{2} d^{MM}_{j+\frac{1}{2}}, \tag{20a}$$

$$f^{lc} = \frac{1}{2}(f_j + f_j^{ul}) + \frac{1}{2}\sigma(r_{j+\frac{1}{2}}, v) \cdot d^{MM}_{j-\frac{1}{2}}, \tag{20b}$$

where $d^{MM}_{j+\frac{1}{2}} = \min \mathrm{mod}(d_j, d_{j+1})$, $d_j = f_{j+1} + f_{j-1} - 2f_j$. In practice, as was done in ref. [10], the paymasters are streng-

thened by choosing a different definition for the curvature measurement definition $d^{MM}_{j+\frac{1}{2}}$, namely

$$d^{M4}_{j+\frac{1}{2}} = \min\text{mod}(4d_j - d_{j+1}, 4d_{j+1} - d_j, d_j, d_{j+1}).$$

Besides, the newly introduced $\sigma(r_{j+\frac{1}{2}}, \nu)$ is defined as:

$$\sigma(r,\nu) = \begin{cases} \kappa(r,\nu), & r \geqslant 0, \\ \beta, & r < 0. \end{cases} \tag{21}$$

β is an experience parameter related to local extrema. However, due to differences in local extrema, the σ function has no unified expression. In the monotonic parts, the new f^{md} and f^{lc} still satisfy (19a) and (19b).

According to the modification in sec. 2.3 and our numerical tests, f^{lc} ultimately has the following expression

$$f^{lc} = \frac{1}{2}(f_j + f^{ul}_j) + \frac{1}{2}d^{MM}_{j-\frac{1}{2}}. \tag{20b′}$$

So the two enlarged intervals are

$$\hat{f}_{j+\frac{1}{2}} \in \left[f_j, f_{j+1}, f^{md} \right], \tag{22a}$$

$$\hat{f}_{j+\frac{1}{2}} \in \left[f_j, f^{ul}, f^{lc} \right]. \tag{22b}$$

Finally, we discuss the accuracy near the local extema. Ref. [10] analyzed the local extrema based on the parabola interpolation. As the local extrema can be tremendously different, there is no unified description for them. But numerical tests [26] have demonstrated that the method is feasible despite a possibly little loss of accuracy near the extrema.

Applying it to the UCD5, we get a 5th order monotonicity-preserving upwind compact difference schemes (m-UCD5).

Here, we summarize the algorithm for $\hat{f}_{j+1/2}$:

(1) According to (7a), calculate the numerical flux $\hat{f}_{j+1/2}$;

(2) If $(\hat{f}_{j+\frac{1}{2}} - f_j)(\hat{f}_{j+\frac{1}{2}} - f^{mp}_b) \leqslant \varepsilon$ holds, then the limiting procedure ends; if not, go to (3);

(3) Calculate (14), (18a), (20b′), and

$$f^{\max}_j = \max(\min(f_j, f_{j+1}, f^{md}_j),\ \min(f_j, f^{ul}_j, f^{lc}_j)),$$

$$f^{\min}_j = \min(\max(f_j, f_{j+1}, f^{md}_j),\ \max(f_j, f^{ul}_j, f^{lc}_j)),$$

$$\hat{f}_{j+\frac{1}{2}} \leftarrow \hat{f}_{j+\frac{1}{2}} + \min\text{mod}\left(f^{\min}_j - \hat{f}_{j+\frac{1}{2}}, f^{\max}_j - \hat{f}_{j+\frac{1}{2}} \right),$$

The minmod function follows the definition in [10], namely

$$\min\text{mod}(z_1, z_2, z_3, \cdots, x_k) = s\min\left(|z_1|, |z_2|, |z_3|, \cdots, |x_k|\right),$$

where

$$s = \frac{1}{2}(\text{sign}(z_1) + \text{sign}(z_2)) \times \left| \frac{1}{2}(\text{sign}(z_1) + \text{sign}(z_3)) \ldots \frac{1}{2}(\text{sign}(z_1) + \text{sign}(z_k)) \right|.$$

3 The Euler equations of gas dynamics

3.1 The Euler equations of gas dynamics and its semi-discrete scheme

The Euler equations of gas dynamics which in the one dimension case, can be written in the following conservative form:

$$\frac{\partial \boldsymbol{U}}{\partial t} + \frac{\partial \boldsymbol{F}(\boldsymbol{U})}{\partial x} = 0, \tag{23}$$

where $\boldsymbol{U} = (\rho, \rho u, \rho E)^{\mathrm{T}}$ is the vector of conservative variables, and the flux is the vector of $\boldsymbol{F}(\boldsymbol{U}) = (\rho u, \rho u^2 + p, (\rho E + p)u)^{\mathrm{T}}$, among them, ρ, u, E and p being the density, the velocity, and the total energy respectively.

The semi-discrete conservative finite difference scheme of (23) can be written as:

$$\frac{\partial \boldsymbol{U}}{\partial t} + \frac{1}{h}(\hat{\boldsymbol{F}}_{j+1/2} - \hat{\boldsymbol{F}}_{j-1/2}) = 0, \tag{24}$$

where $\hat{\boldsymbol{F}}_{j+1/2}$ is the numerical flux function.

If

$$\frac{1}{h}(\hat{\boldsymbol{F}}_{j+1/2} - \hat{\boldsymbol{F}}_{j-1/2}) = \left(\frac{\partial \boldsymbol{F}}{\partial x} \right)_j + O(h^k), \tag{25}$$

this scheme is the k th order scheme.

3.2 Application of the scheme to the Euler equations

In this paper, we extend the scheme to solve the Euler equations in two forms, i.e., the component-wise m-UCD5 and characteristic-wise m-UCD5. The following is the detailed description.

Form1: Use the Steger-Warming flux vector splitting (or other flux vector splitting such as Van Leer FVS) method to split the fluxes into a positive part and a negative part, i.e., $\boldsymbol{F} = \boldsymbol{F}^+ + \boldsymbol{F}^-$. Then use the scheme to solve the Euler equations in a component by component manner, resulting in a scheme called component-wise m-UCD5.

Form2: It is usually advisable to use the more costly but

much sounder approach based on the characteristic decomposition. Although the scheme is compact, there is no significant difference. The characteristic-wise m-UCD5 scheme consists of the following steps:

(1) Use the Steger-Warming flux vector splitting method to split the fluxes into a positive part and a negative part, i.e., $\boldsymbol{F} = \boldsymbol{F}^+ + \boldsymbol{F}^-$. Here we can also use other flux vector splitting methods such as Van Leer FVS method.

(2) At each fixed $x_{j+1/2}$, the average state $\boldsymbol{U}_{j+1/2}$ is computed by the simple mean or the Roe mean.

(3) The eigenvalues $\lambda^{(i)}_{j+1/2}(i=1,2,3)$, the left eigenvectors $\vec{l}^{(i)}_{j+1/2}(i=1,2,3)$ and the right eigenvectors $\vec{r}^{(i)}_{j+1/2}$ $(i=1,2,3)$ are computed in terms of $\boldsymbol{U}_{j+1/2}$.

(4) The local characteristic decompositions of the flux functions at x_m are computed using:

$$w^{+(i)}_m = \vec{l}^{(i)}_{j+1/2}\cdot \boldsymbol{F}^+_m,\ i=1,2,3;\ m=j-1,\cdots,j+2,$$

$$w^{-(i)}_m = \vec{l}^{(i)}_{j+1/2}\cdot \boldsymbol{F}^-_m,\ i=1,2,3;\ m=j+2,\cdots,j-1.$$

Besides, the numerical flux of upwind point $\hat{\boldsymbol{F}}^+_{j-\frac{1}{2}}$ and $\hat{\boldsymbol{F}}^-_{j+\frac{3}{2}}$ should be re-decomposited locally at $j+1/2$, resulting in $\hat{w}^{+(i)}_{j-\frac{1}{2}}$ and $\hat{w}^{-(i)}_{j+\frac{3}{2}}$.

(5) Calculate

$$\hat{w}^{+(i)}_{j+\frac{1}{2}} = \frac{5}{3}\cdot\left[\left(\frac{3w^{+(i)}_{j-1}+47w^{+(i)}_j+11w^{+(i)}_{j+1}-w^{+(i)}_{j+2}}{60}\right)-\frac{2}{5}\hat{w}^{+(i)}_{j-\frac{1}{2}}\right],$$

$$\hat{w}^{-(i)}_{j+\frac{1}{2}} = \frac{5}{3}\cdot\left[\left(\frac{3w^{-(i)}_{j+2}+47w^{-(i)}_{j+1}+11w^{-(i)}_j-w^{-(i)}_{j-1}}{60}\right)-\frac{2}{5}\hat{w}^{-(i)}_{j+\frac{3}{2}}\right],$$

(6) Execute the limiting procedures.

(7) And transform back into physical space to get $\hat{\boldsymbol{F}}_{j+1/2} = \hat{\boldsymbol{F}}^+_{j+1/2} + \hat{\boldsymbol{F}}^-_{j+1/2}$.

4 Numerical results

In this section, we use the new scheme to solve some 1D and 2D tests, focusing on comparing it with the original UCD5 and the classical WENO5.

4.1 Example 1: Advection of an initial profile with discontinuities

In order to compare the resolution and computational load with the classical scheme WENO5, we consider the test case of the advection of an initial profile composed of a Gaussian wave, a square wave, a triangular wave and an ellipse wave.

The problem is

$$\text{equation: } \frac{\partial u}{\partial t}+\frac{\partial u}{\partial x}=0,$$

initial condition: on the interval [−1,1], the initial conditions are:

$$\begin{cases} u_0(x)=\exp(-\log(2)(x+0.7)^2/0.0009), & \text{if } -0.8\leqslant x\leqslant -0.6,\\ u_0(x)=1, & \text{if } -0.4\leqslant x\leqslant -0.2,\\ u_0(x)=1-\left|10(x-0.1)\right|, & \text{if } 0\leqslant x\leqslant 0.2,\\ u_0(x)=[1-100(x-0.5)^2]^{1/2}, & \text{if } 0\leqslant x\leqslant 0.2\\ u_0(x)=0, & \text{otherwise.}\end{cases}$$

Figure 3 shows the results obtained by the m-UCD5 and WENO5. The m-UCD5 scheme obviously gives a better result compared with WENO5.

Table 2 compares the CPU times needed for the numerical simulation by using m-UCD5 and WENO5. This table shows that the time needed for m-UCD5 is less, and the CPU time of m-UCD5 is only 62% of that of WENO5.

4.2 Example 2: Sod problem

This is a classical test. The governing equations are the one-dimensional Euler equations and the initial conditions are

$$(\rho,u,p)=\begin{cases}(1,0,1), & \text{if } x<0.5,\\ (0.125,0,0.1), & \text{if } x\geqslant 0.5,\end{cases}$$

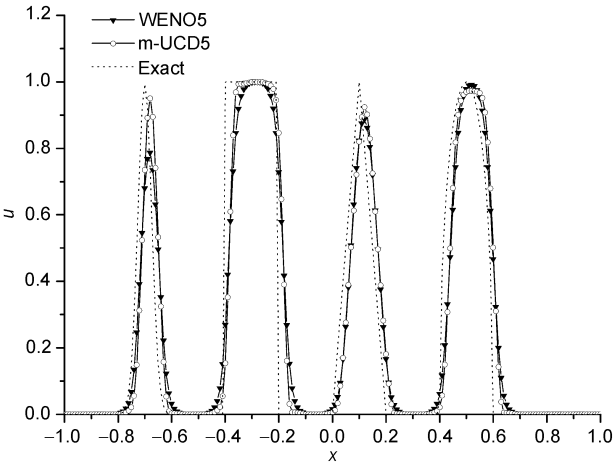

Figure 3 The results obtained by the m-UCD5 and WENO5.

Table 2 The CPU times needed for the m-UCD5 and WENO5 (2000 time steps)

Method	CPU time (ms)
m-UCD5	221.755
WENO5	353.396

The solution is advanced in time up to $t = 0.14$ on the computational domain $x \in [0,1]$. And the time step is determined by

$$\Delta t = \mathrm{CFL} \cdot \frac{h}{\max_j(|u|_j + a_j)},$$

where CFL equals 0.2 and the mesh number is N=100.

Numerical results computed by the 5th order monotonicity-preserving upwind compact difference scheme (m-UCD5) and the original 5th order upwind compact difference scheme (UCD5) are shown in Figure 4. Obviously the new scheme is free of the spurious oscillations while the original scheme is not. So we can say that the new scheme produces a good result.

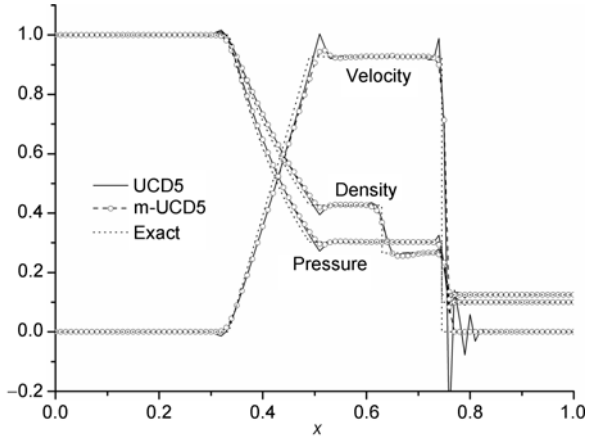

Figure 4 Distributions of density, velocity and pressure. Component-wise. N=100.

Besides, the density, velocity and pressure distribution obtained by WENO5 and m-UCD5 are shown in Figures 5–7, respectively, where Figures 5(b) and 5(c) are enlarged portions of Figure 5(a), while Figures 6(b) and 6(c) are of Figure 6(a), and Figures 7(b) and 7(c) are of Figure 7(a).

By comparing these figures, we can say that the new scheme has deleted the drawback of non-physical oscillations of the original UCD5. Furthermore, the new scheme produces a better solution while the computational load is less than the classical WENO5's.

Finally, we give the result obtained by the characteristic-wise m-UCD5 which is the more costly but much sounder approach based on the characteristic decomposition (see Figure 8). From this figure, it is evident that the characteristic-wise m-UCD5 achieves a higher resolution in the numerical results than the component-wise m-UCD5.

4.3 Example 3: Shu-Osher problem

This problem represents that Mach 3 shock interacts with a density disturbance which will generate a flow field with

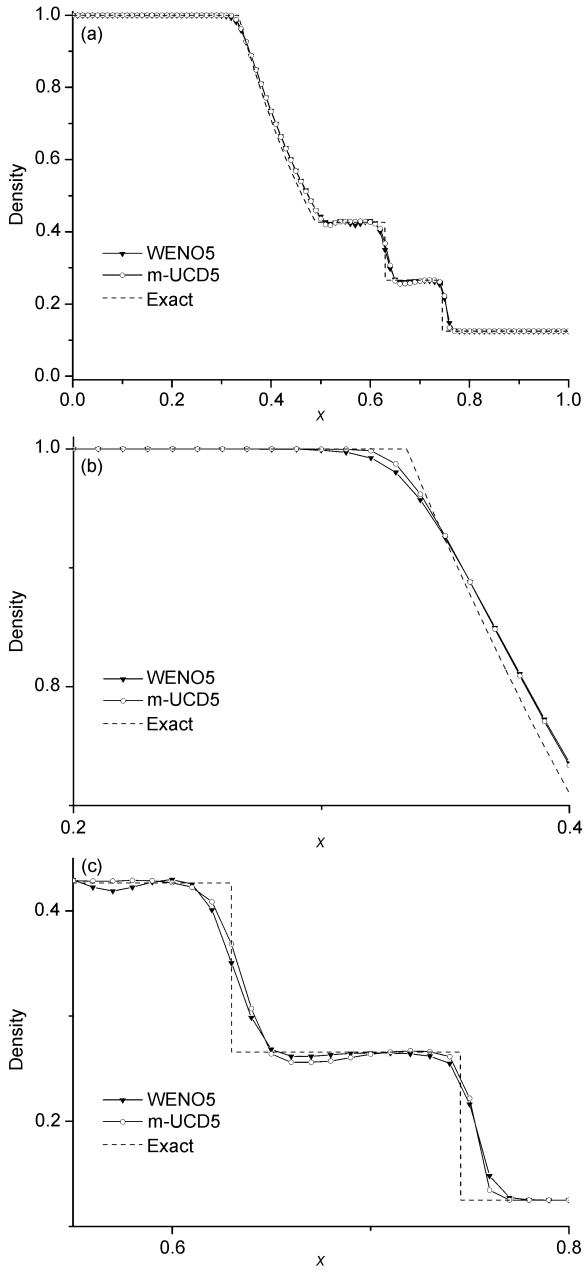

Figure 5 Distribution of density. Component-wise. N=100.

both smooth structure and discontinuities. The governing equation is the one-dimensional Euler equations and the initial conditions are

$$(\rho, u, p) = \begin{cases} (3.857143, 2.629369, 10.333333), & \text{if } x < -4, \\ (1 + 0.2\sin(5x - 5), 0, 1), & \text{if } x \geqslant -4. \end{cases}$$

The solution is advanced in time up to $t = 1.8$ on the computational domain $x \in [-5,5]$.

The time step is determined by

$$\Delta t = \mathrm{CFL} \cdot \frac{h}{\max_j(|u|_j + a_j)}.$$

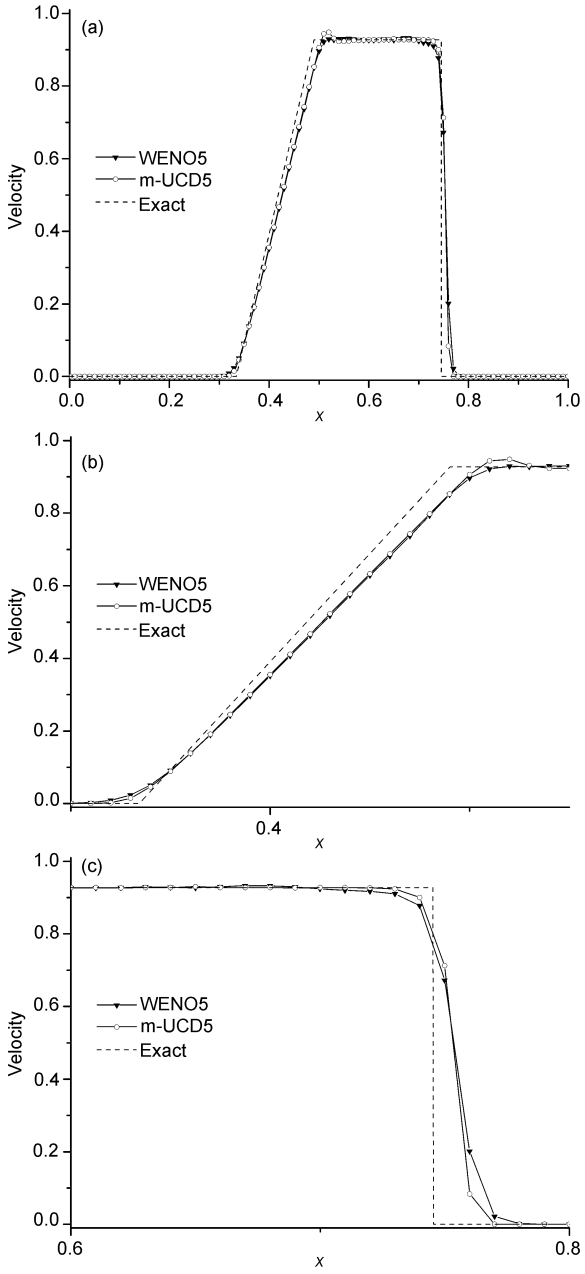

Figure 6 Distribution of velocity. Component-wise. N=100.

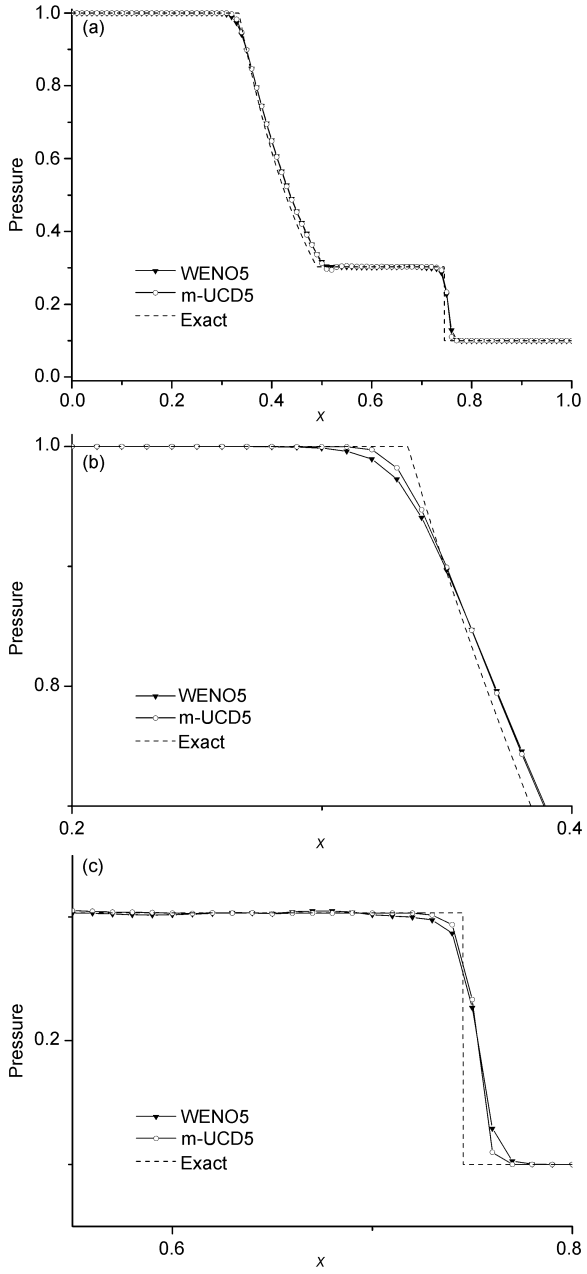

Figure 7 Distribution of pressure. Component-wise. N=100.

where the CFL number equals 0.2.

The original UCD5 scheme is not robust enough to calculate this problem while the new component-wise m-UCD5 scheme produces a rather good solution shown in Figure 9. In order to compare the new scheme with WENO5, the result obtained by WENO5 is also presented in Figure 9. Figure 9(b) is an enlarged portion of Figure 9(a) and the grid number is N=200. It is obvious that the new scheme does achieve a better result than the WENO5 scheme.

Figure 10 gives the results obtained by component-wise m-UCD5 and WENO5 while the grid number is N=400.

Again, we give the result obtained by the characteristic-wise m-UCD5 (see Figure 11). It achieves a higher resolution in the numerical results than the component-wise m-UCD5 is again demonstrated.

Note that for this problem, the "exact" solution is obtained by WENO5 using 4000 gird points, since the real exact solution is not known.

4.4 Example 4: Double Mach Reflection problem

This is a classical two-dimensional test case for high resolution schemes [27]. The computational domain for this problem is [0,4]×[0,1] and a plate lies on the bottom of the computational domain starting form x=1/6. Initially, a right-moving Mach 10 shock is positioned across (x=1/6, y=0)

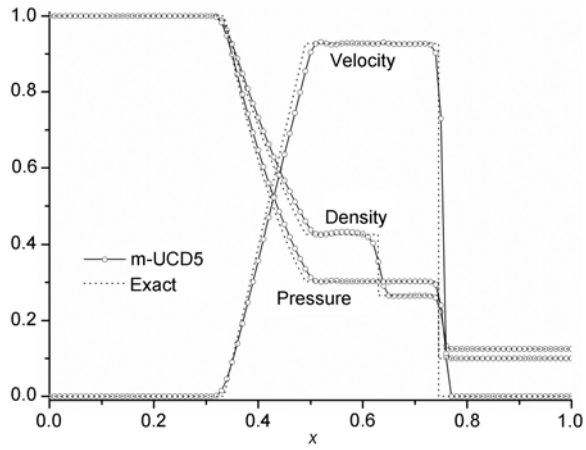

Figure 8 Distributions of density, velocity and pressure. Characteristic-wise. N=100.

and makes a 60° angle with the x-axis (see in Figure 12).

The solution is advanced in time up to $t = 0.2$. And the time step is computed according to

$$\Delta t = \mathrm{CFL} \cdot \frac{\Delta t_x \Delta t_y}{\Delta t_x + \Delta t_y},$$

where

$$\Delta t_x = \frac{\Delta x}{\max_{j,k}(|u|_{j,k} + a_{j,k})}.$$

The CFL number is 0.2.

The original scheme is again unable to produce a result for this problem. Figure 13 gives the results obtained by component-wise m-UCD5 and WENO5 while Figures 13(c) and 13(d) are enlarged portions of Figures 13(a) and 13(b), respectively.

The figures show that the new scheme achieves a high resolution in the numerical results, especially in the region near the Mach stems where the new scheme can capture the rollup of the slip line more clearly. And we can say that the dissipation of the new scheme is much smaller than the WENO5's.

However, the result obtained by the component-wise m-UCD5 shows some obvious numerical oscillations which can be easily gotten rid of by using the characteristic-wise m-UCD5 (See Figure 14). Obviously the characteristic-wise m-UCD5 achieves a clear and clean result but introduces more dissipation for the slip line.

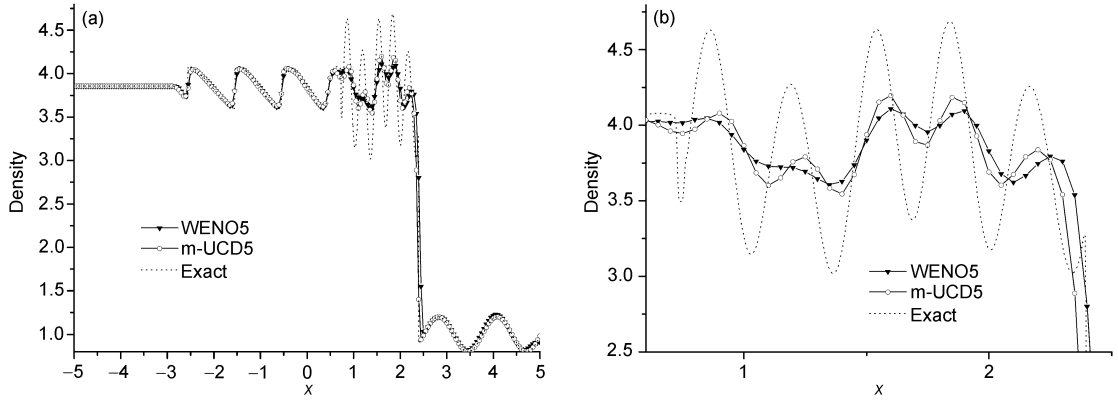

Figure 9 Distributions of density. Component-wise. N=200.

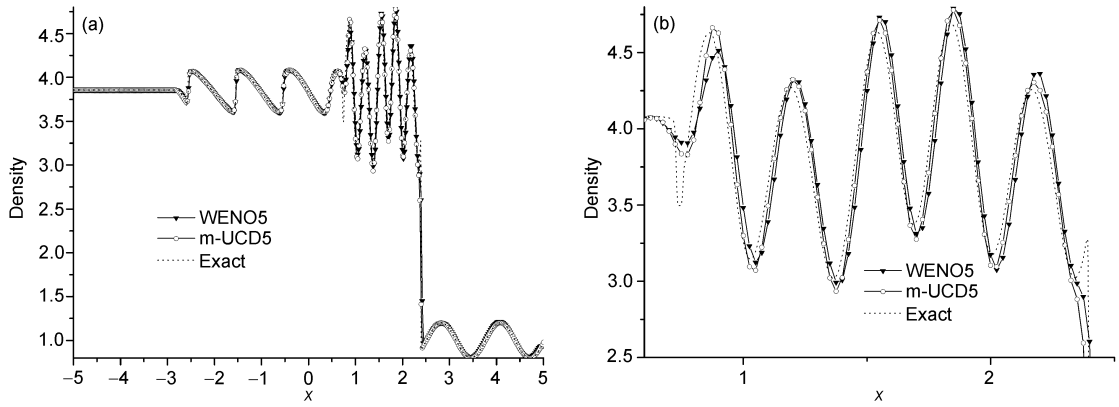

Figure 10 Distributions of density. Component-wise. N=400.

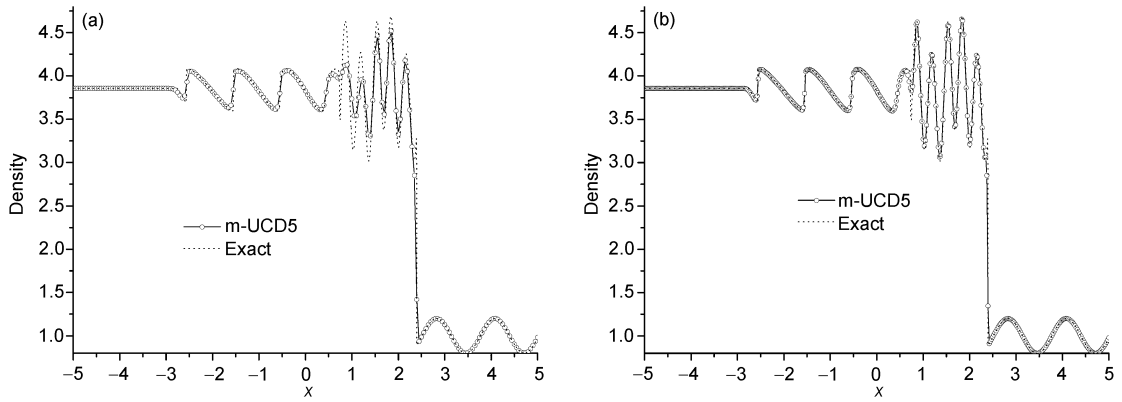

Figure 11 Distributions of density. Characteristic-wise. (a) N=200; (b) N=400.

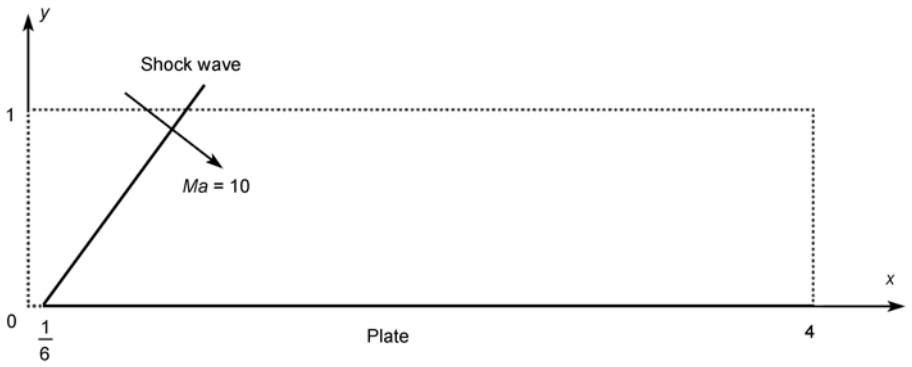

Figure 12 The schematic drawing of Double Mach Reflection.

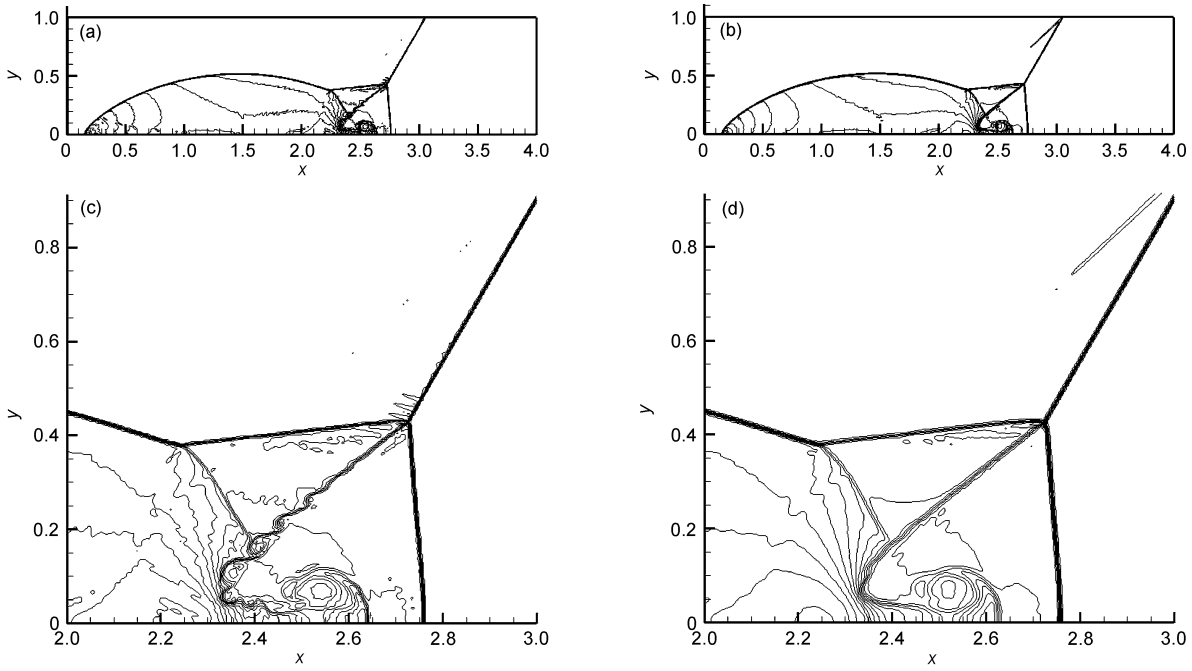

Figure 13 Density contours of the Double Mach Reflection problem (from 1.731 to 20.92 with 30 equally spaced contours). t=0.2. 960×240. Component-wise. (a) m-UCD5; (b) WENO5; (c) enlarged portion of (a); (d) enlarged portion of (b).

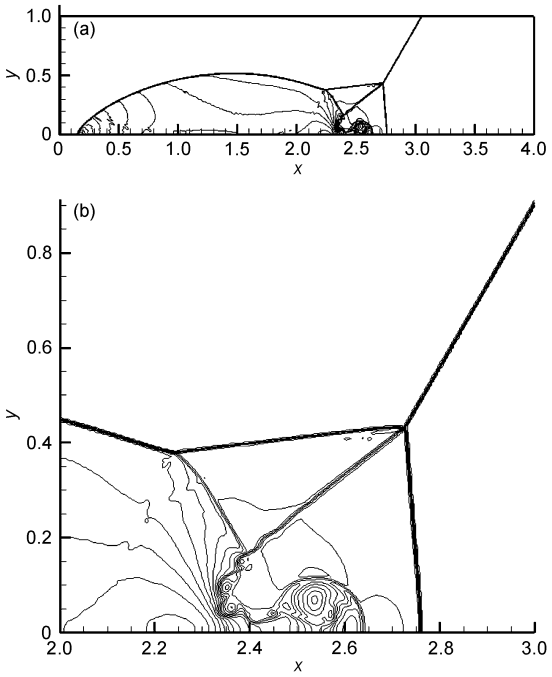

Figure 14 Density contours of the Double Mach Reflection problem (from 1.731 to 20.92 with 30 equally spaced contours). t=0.2. 960×240. Characteristic-wise.

5 Conclusion

In this paper, a 5th order monotonicity-preserving upwind compact difference scheme (m-UCD5) is proposed. Numerical results demonstrate that compared with the classical 5th order WENO difference scheme, the new difference scheme is simple and is small in diffusion and computation load. Besides, we offer two forms of the new scheme, i.e., the component-wise m-UCD5 and characteristic-wise m-UCD5. The application of the new scheme to the N-S/Euler equations has yielded good numerical results.

Thanks go to the Supercomputing Center of Chinese Academy of Sciences (SCCAS) and Shanghai Supercomputer Center (SSC) for providing the computing time. This work was supported by the National Natural Science Foundation of China (Grant Nos. 110632050, 10872205), the National Basic Research Program of China (Grant No. 2009CB724100), and Projects of CAS INFO-115-B01.

1 Harten A. High resolution schemes for hyperbolic conservation laws. J Comput Phys, 1983, 59: 357–393
2 Toro E. Riemann solvers and numerical methods for fluid dynamics. Berlin: Springer, 1997
3 Sweby P K. High resolution schemes using flux limiters for Hyperbolic conservation laws. SIAM J Numer Anal, 1984, 21: 995–1011
4 Van Leer B. Towards the ultimate conservative difference scheme V. A second order sequel to Godunov's method. J Comput Phys, 1979, 32: 101–136
5 Zhang H X. Non-oscillatory and non-free-parameter dissipation difference scheme (in Chinese). Acta Aerodyn Sin, 1988, 6: 143–165
6 Harten A, Engquist B, Osher S, et al. Uniformly high order accurate essentially non-oscillatory shock-capturing schemes III. J Comput Phys, 1987, 71: 231–303
7 Serna S, Marquina A. Power ENO methods: A fifth-order accurate weighted power ENO method. J Comput Phys, 2004, 194: 632–658
8 Jiang G S, Shu C W. Efficient implementation of weighted ENO schemes. J Comput Phys, 1996, 126: 202–228
9 Shu C W. TVB uniformly high-order schemes for conservation laws. Math Comput, 1987, 49: 105–121
10 Suresh A, Huynh H T. Accurate monotonicity-preserving schemes with Runge-Kutta time stepping. J Comput Phys, 1997, 136: 83–99
11 Lele S K. Compact finite difference schemes with spectral-like resolution. J Comput Phys, 1992, 103: 16–42
12 Fu D X, Ma Y W. High resolution schemes, Computational Fluid Dynamics Review. Hafez M, Oshima K, Eds. New York: John Willey & Sons, 1995. 234–250
13 Halt D W, Agarwal R K. Compact higher order characteristic-based Euler solver for unstructured grids. AIAA J, 1992, 30: 1993–1999
14 Cockburn B, Shu C W. Nonlinearly stable compact schemes for shock calculations. SIAM J Numer Anal, 1994, 31: 607–627
15 Ravichandran K S. High order KFVS algorithms using compact upwind difference operators. J Comput Phys, 1997, 130: 161–173
16 Adams N A, Shariff K. A high-resolution hybrid compact-ENO scheme for shock-turbulence interaction problems. J Comput Phys, 1996, 127: 27–51
17 Pirozzoli S. Conservative hybrid compact-WENO schemes for shock-turbulence interaction. J Comput Phys, 2002, 178: 81–117
18 Ren Y X, Liu M E, Zhang H X. A characteristic-wise hybrid compact-WENO scheme for solving hyperbolic conservation laws. J Comput Phys, 2003, 192: 365–386
19 Deng X, Zhang H. Developing high-order weighted compact nonlinear schemes. J Comput Phys, 2000, 165: 22–44
20 Ma Y W, Fu D X. Fourth order accurate compact scheme with group velocity control (GVC). Sci China Ser A-Math Phys Astron, 2001, 44: 1197–1204
21 Shu C W, Osher S. Efficient implementation of essentially nonoscillatory schemes. J Comput Phys, 1989, 83: 32–78
22 Fu D X, Ma Y W. A high order accurate difference scheme for complex flow fields. J Comput Phys, 1997, 134: 1–15
23 Fu D X, Ma Y W. Computational Fluid Dynamics (in Chinese). Beijing: Higher Education Press, 2002
24 Daru V, Tenaud C. High order one-step monotonicity-preserving schemes for unsteady compressible flow calculations. J Comput Phys, 2004 193: 563–594
25 Waterson N P, Deconinck H. Design principles for bounded higher-order convection schemes-a unified approach. J Comput Phys, 2007, 224: 182–207
26 Balsara D S, Shu C W. Monotonicity preserving weighted essentially nonoscillatory schemes with increasingly high order of accuracy. J Comput Phys, 2000, 160: 405–452
27 Woodward P, Colella P. Numerical simulations of two-dimensional fluid flow with strong shocks. J Comput Phys, 1984, 54: 115–173